Atmos. Meas. Tech., 19, 1763–1781, 2026
https://doi.org/10.5194/amt-19-1763-2026

Atmospheric Measurement Techniques
Open Access
EGU

Evaluation of calibration strategies for accurate $\delta^{13}CH_4$ measurements in dry and humid air

Ji Li[1,2,3], Xuguang Chi[1,2], Aijun Ding[1,2,3], Weimin Ju[4], Yongguang Zhang[4,5], Jing M. Chen[6,7], and Huilin Chen[1,2,3]

[1]Joint International Research Laboratory of Atmospheric and Earth System Sciences, School of Atmospheric Sciences, Nanjing University, Nanjing, China
[2]Jiangsu Provincal Collorative Innovation Center of Climate Change, Nanjing, China
[3]Frontiers Science Center for Critical Earth Material Cycling, Nanjing University, Nanjing, 210023, China
[4]Jiangsu Provincial Key Laboratory of Geographic Information Science and Technology, Key Laboratory for Land Satellite Remote Sensing Applications of Ministry of Natural Resources, School of Geography and Ocean Science, Nanjing University, Nanjing, Jiangsu, China
[5]Jiangsu Center for Collaborative Innovation in Geographical Information Resource Development and Application, International Institute for Earth System Sciences, Nanjing University, Nanjing, Jiangsu 210023, China
[6]School of Geographical Science, Key Laboratory for Humid Subtropical Eco-Geographical Processes of the Ministry of Education, Fujian Normal University, Fuzhou 350008, China
[7]Department of Geography and Planning, University of Toronto, Toronto, ON M5S 3G3, Canada

Correspondence: Huilin Chen (huilin.chen@nju.edu.cn)

Received: 11 November 2025 – Discussion started: 19 November 2025
Revised: 3 March 2026 – Accepted: 4 March 2026 – Published: 11 March 2026

Abstract. Accurate determination of the methane isotopic composition ($\delta^{13}CH_4$) is essential for attributing emission sources of methane (CH_4). However, for measurements with optical instruments, spectral interference from water vapor and instrumental drift often introduce substantial biases in $\delta^{13}CH_4$ measurements, particularly for humid air measurements. Although multiple calibration strategies exist, a systematic evaluation of their performance under diverse field conditions remains lacking. Here, we evaluate two calibration strategies for a cavity ring-down spectrometer: a delta-based calibration for $\delta^{13}CH_4$ and an isotopologue-specific calibration for $^{12}CH_4$ and $^{13}CH_4$. We performed laboratory experiments over a water vapor range of 0.15 %–4.0 % to establish empirical correction functions, quadratic for $^{12}CH_4$ and $^{13}CH_4$, and linear for $\delta^{13}CH_4$, to remove humidity-induced biases. These correction functions were then applied to field measurements in both dried air at the SORPES stie and humid air at the Jurong site. At the SORPES site where air samples were dried using a Nafion™ dryer, the mean difference in $\delta^{13}CH_4$ between the two strategies was ~ 0.29 ‰. In contrast, for humid air at the Jurong site, significant inter-method difference ($\Delta\delta^{13}CH_4$) was observed, with which exhibiting a strong correlation with $1/CH_4$, indicating non-linear spectral effects are most pronounced at lower CH_4 concentrations and compromise the performance of delta-based calibration. Notably, only the isotopologue-specific calibration, coupled with an explicit water vapor correction, delivered stable and accurate $\delta^{13}CH_4$ measurements across all conditions. This work underscores the need for robust calibration strategies to minimize bias in CH_4 isotopic composition measurements.

1 Introduction

Methane (CH_4) is a potent greenhouse gas that plays a key role in climate change, contributing approximately 16.4 % of total anthropogenic radiative forcing (Patra and Khatri, 2022). Its global warming potential is about 28 times greater than that of carbon dioxide (CO_2) over a 100-year time horizon, making CH_4 a critical target for near-term climate mitigation (Forster et al., 2021; Nisbet et al., 2020; Van Dingenen et al., 2018; Shindell et al., 2012; Ipcc, 2007). The

primary sources of CH_4 emissions are direct anthropogenic activities (e.g., agriculture, waste, fossil fuels, and biomass burning), and natural and indirect anthropogenic sources, including wetlands, inland waters, and geological seepage. In contrast, its removal from the atmosphere is mainly governed by oxidation with hydroxyl radicals (OH) (Kirschke et al., 2013; Olivier and Berdowski, 2021; Saunois et al., 2020). However, substantial uncertainties remain in these estimates: 20 %–35 % for anthropogenic sources, $\sim$ 50 % for wetlands and biomass burning, up to 100 % for inland waters and geological sources, and 10 %–20 % for the OH sink (Saunois et al., 2025). To constrain budgets and design effective reduction strategies, it is essential to distinguish between its diverse emission sources.

The carbon isotopic composition of CH_4 ($\delta^{13}CH_4$) provides valuable constraints on tracking emission sources (Nisbet et al., 2016; Rice et al., 2016; Schaefer et al., 2016), as microbial, thermogenic, and pyrogenic origins exhibit distinct isotopic signatures (Levin et al., 1993; Bakkaloglu et al., 2022; Ehleringer and Osmond, 1989). $\delta^{13}CH_4$-based analysis enables classification of emission types and supports quantitative estimation of CH_4 emissions on regional to global scales (De Groot, 2004; Saunois et al., 2020; Lan et al., 2021). However, these applications critically depend on high-precision isotopic measurements, since even small observational biases can propagate into large errors in inferred source signatures (Iaea, 2024; Defratyka et al., 2025; France et al., 2022).

Conventionally, $\delta^{13}CH_4$ has been measured using isotope ratio mass spectrometry (IRMS), which provides high precision measurements (≤ 0.1 ‰) but requires labor-intensive sampling and lacks continuous coverage (Miller et al., 2002; Schaefer et al., 2006; Röckmann et al., 2016). Recent advances in laser-based spectroscopy, particularly cavity ring-down spectroscopy (CRDS) and quantum cascade laser absorption spectroscopy (QCLAS), have enabled in situ and automated $\delta^{13}CH_4$ monitoring (Rella et al., 2015; Tuzson et al., 2008). While these techniques offer advantages over conventional IRMS, their measurement accuracy is challenged by spectroscopic interferences, such as water vapor, and by the choice of calibration strategies. This is true whether $\delta^{13}CH_4$ is adjusted directly or is derived from isotopologue-specific calibrations, as highlighted in subsequent evaluations (Griffith, 2018; Hoheisel et al., 2019; Saboya et al., 2022).

Water vapor affects measured CH_4 mole fractions through dilution and spectral interference, thereby introducing systematic biases in isotopologue-based measurements (Chen et al., 2010; Hoheisel et al., 2019; Saboya et al., 2022). Consequently, whether the sampled air is dried prior to analysis critically affects the accuracy of $\delta^{13}CH_4$ measurements, a factor that becomes particularly important in humid environments. In addition, two primary calibration strategies have been developed to retrieve $\delta^{13}CH_4$ from laser-based spectroscopic observations (Wen et al., 2013; Griffith, 2018; Griffith et al., 2012; Flores et al., 2017; Tans et al., 2017). One is a direct correction of $\delta^{13}CH_4$ (hereafter, *delta-based correction*), which is relatively straightforward but may retain residual artifacts linked to CH_4 concentration (Wen et al., 2013; Pang et al., 2016; Griffith et al., 2012; Braden-Behrens et al., 2017; Flores et al., 2017). Another one is isotopologue-specific correction for $^{12}CH_4$ and $^{13}CH_4$ (hereafter, *isotopologue-specific correction*), in which $\delta^{13}CH_4$ is derived from independently corrected isotopologue concentrations, thereby reducing concentration-dependent biases (Griffith, 2018; Wen et al., 2013).

As water vapor remains a dominant limitation for accurate $\delta^{13}CH_4$ measurement, physical drying to approximately $<$ 0.1 % H_2O (dew point ≈ -25 °C) is generally recommended to obtain high-precision $\delta^{13}CH_4$ measurements at the sub-per-mil level (Rella et al., 2015). Laboratory studies demonstrated a quadratic CH_4–H_2O relationship, indicating that water vapor affects CH_4 through both dilution and spectral interference (Chen et al., 2010; Rella et al., 2013), and a cross-sensitivity of ~ 0.54 ‰ per 1 % H_2O within 0.15 %–1.5 % H_2O (Hoheisel et al., 2019). In comparison, Saboya et al. (2022) applied a linear $\delta^{13}CH_4$ correction over 0 %–2.2 % H_2O and found CH_4 mole fractions to be unaffected by water vapor within this range, while Chen et al. (2010) reported a clear quadratic dependence across 0.6 %–6 % H_2O. Moreover, explicit correction functions for the individual isotopologues ($^{12}CH_4$ and $^{13}CH_4$) remain lacking, and the $\delta^{13}CH_4$ corrections vary widely in form, highlighting the need for more robust approaches. Both calibration strategies ideally rely on multi-point calibration using reference gases that span the targeted range, either in mole fractions of $^{12}CH_4$ and $^{13}CH_4$ (for isotopologue-specific calibration) or in $\delta^{13}CH_4$ (for delta-based calibration) (Wen et al., 2013; Griffith, 2018), but practical limitations persist. Delta-based correction is constrained by scarce isotopic standards (Griffith, 2018) and prone to concentration-dependent biases (Wen et al., 2013; Griffith, 2018), while isotopologue-specific correction can reduce such concentration dependence but lacks well-established water correction functions for $^{12}CH_4$ and $^{13}CH_4$. These methodological gaps are particularly critical in humid environments, where water vapor effects are often large.

In this study, we aim to evaluate isotopologue-specific and delta-based calibration strategies for obtaining accurate $\delta^{13}CH_4$ measurements for both dry and humid air. To achieve this, we conducted water vapor laboratory experiments to derive empirical correction functions for $^{12}CH_4$, $^{13}CH_4$, and $\delta^{13}CH_4$. These corrections were then applied to field measurements to assess the accuracy of both calibration strategies for measurements in both dry and humid air.

2 Materials and Methods

2.1 The $\delta^{13}CH_4$ analyzer

The δ^{13}C-CH_4 analyzer used in this study was a G2201-i instrument manufactured by Picarro Inc. (Santa Clara, CA, USA). All laboratory experiments and field measurements reported here were performed using the same G2201-i analyzer, although the field measurements were performed during different campaigns in different years (2018, 2022, and 2025). This instrument is based on the cavity ring-down spectroscopy (CRDS) technique, which enables real-time measurements of CH_4 and CO_2 isotopologues ($^{12}CH_4$, $^{13}CH_4$, $^{12}CO_2$, $^{13}CO_2$). CRDS quantifies gas absorption by measuring the exponential decay rate of light intensity in a high-reflectivity optical cavity, providing high sensitivity and strong resistance to external interference (Crosson, 2008; Berden and Engeln, 2009; Crosson et al., 2002; Wahl et al., 2006). Here, we evaluate observations of both CH_4 mole fractions and $\delta^{13}CH_4$ values derived from $^{12}CH_4$ and $^{13}CH_4$ measurements.

The instrument is equipped with a dual-laser module that allows automatic switching between CH_4 and CO_2 isotopologue measurements. During experiments covering a humidity range of 0 %–4.0 %, the cavity temperature and pressure remained highly stable (45.000 ± 0.001 °C and 197.317 ± 0.084 hPa, respectively). The analyzer applies an internal, empirically parameterized water-vapor interference correction based on the measured H_2O absorption signal (peak75), which is non-linear and includes a quadratic term, as described in the G2201-i user manual. The analyzer includes an internal water vapor correction algorithm that compensates for humidity effects for the calculation of $\delta^{13}CH_4$. According to the manufacturer's white paper, this correction is internally applied to the $^{12}CH_4$ signal before computing $\delta^{13}CH_4$, using an empirically derived function to adjust for H_2O-induced spectral interference (Rella, 2012). In this study, all water-vapor correction functions were derived from the raw (uncorrected) outputs. All subsequent analyses were performed using raw $^{12}CH_4$, $^{13}CH_4$, and $\delta^{13}CH_4$ values corrected offline with the empirical water-vapor correction functions developed here. Manufacturer-corrected outputs were not used in the calibration workflow to avoid potential double correction. As a result, $\delta^{13}CH_4$ values are indirectly adjusted for humidity, whereas the raw $^{12}CH_4$ and $^{13}CH_4$ mole fractions remain uncorrected and represent humid-air concentrations.

2.2 Experimental design and measurement system

2.2.1 Water vapor correction

To quantify and correct for the influence of water vapor on the $\delta^{13}CH_4$ measurements, we performed a water vapor laboratory experiment using a Picarro G2201-i analyzer (Fig. 1a), following a modified setup from Rella et al. (2013). A cotton filter soaked with deionized water was placed at the inlet to gradually humidify the sample stream, forming an artificially humidified phase to derive empirical water vapor correction functions for $^{12}CH_4$, $^{13}CH_4$, and $\delta^{13}CH_4$. The analyzer continuously sampled a reference gas (Ref0, Table 1) at a flow rate of ~ 45 mL min^{-1} for approximately six hours, during which water vapor mole fraction decreased from ~ 4.0 % to ~ 0.1 %. Over the entire experiment, the instrument drift between the two dry-reference periods was 1.8 ppb (0.092 %) for $^{12}CH_4$, 0.02 ppb (0.095 %) for $^{13}CH_4$, and 0.262 ‰ for $\delta^{13}CH_4$ (Fig. 2). Empirical relationships between measured signals and H_2O concentration were then derived. For $^{12}CH_4$ and $^{13}CH_4$, second-order polynomial fits were applied (Chen et al., 2010; Rella et al., 2013), while $\delta^{13}CH_4$ was corrected using a linear regression (Hoheisel et al., 2019). These correction functions were subsequently applied to both reference and field measurements to remove H_2O-induced spectral interference.

The main humidity-response experiment was conducted once in this study. As no repeated humidity tests were performed over time, we cannot assess the temporal stability and reproducibility of the fitted correction functions. For long-term applications, periodic validation and, if necessary, re-derivation of the correction functions are recommended.

2.2.2 Field observations

The $\delta^{13}CH_4$ measurement system was deployed at two sites in the Yangtze River Delta (Fig. 1b, c; Table 2). The Station for Observing Regional Processes of the Earth System (SORPES) station, located on the Xianlin campus of Nanjing University (118°57′10″ E, 32°07′14″ N; ~ 40 m a.s.l.), represents a regional background site influenced by large-scale anthropogenic emissions (Ding et al., 2016). The Jurong station (31°48′24.59″N, 119°13′2.15″E; ~ 15 m a.s.l.) is situated in an irrigated rice paddy and characterizes an agricultural ecosystem under a subtropical monsoon climate (Dai et al., 2019; Li et al., 2020).

At both sites, ambient CH_4 and $\delta^{13}CH_4$ were recorded at 0.5 Hz and aggregated to 5-min means. Reference gases were introduced every six hours to ensure accuracy while conserving calibration gases. Humidity conditions contrasted strongly between two sites: SORPES used a Nafion™ membrane dryers (Perma Pure, USA) to maintain stable H_2O (0.04 %–0.40 %), whereas Jurong operated without drying, resulting in elevated H_2O (0.93 %–3.5 %) consistent with the paddy environment. Calibration approaches also differed. Table 1 describes the compositions and assigned true values of the reference gases (Ref1–Ref3) and working standard gases (WS1–WS5). At Jurong, ambient measurements of CH_4 mole fractions were calibrated using a two-point linear correction based on WS1 and WS3. $\delta^{13}CH_4$ was calibrated using the same two reference gases via the linear delta-based calibration (Eq. 8). WS1 and WS3 span a wide CH_4 range, but exhibit a relatively narrow $\delta^{13}CH_4$ range (Ta-

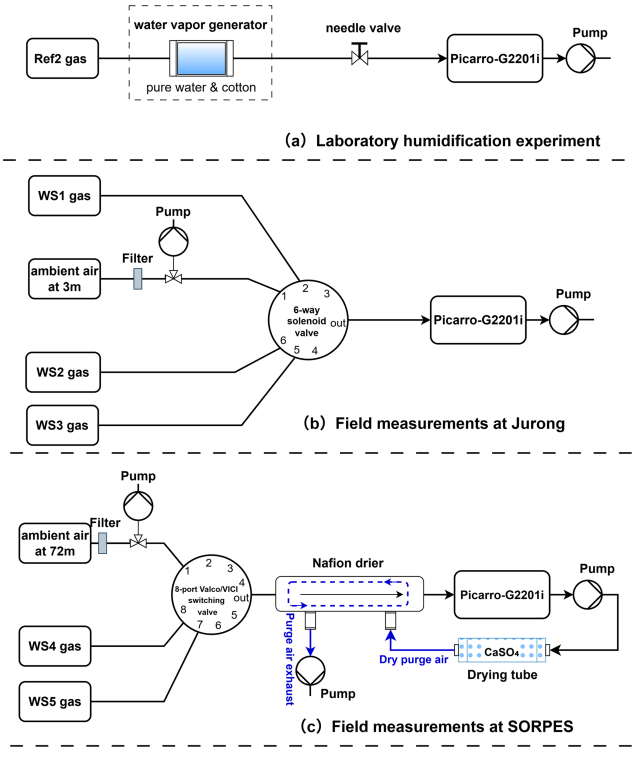

Figure 1. Laboratory and field setups for CH_4 and δ^{13} CH_4 measurements using a Picarro G2201-i analyzer. **(a)** Laboratory setup for deriving the water vapor correction function using humidified Ref2 gas. **(b)** Field setup at the Jurong site using WS1–WS3 and ambient air at 3 m above the ground, streams selected via a solenoid valve. **(c)** Field setup at the SORPES site with WS4–WS5 and ambient air sampled at 72 m above the ground, equipped with a Nafion™ dryer. Note that a 6-way solenoid valve was used at Jurong, whereas an 8-port Valco or VICI switching valve was used at SORPES.

ble 1). At SORPES, WS4 and WS5 were used to determine the calibration slope applied throughout the observation period, whereas WS5 served as a single-point reference to correct instrument drift.

2.2.3 Reference gas measurements

Reference gases were measured in the laboratory and at both field sites to evaluate the performance of the calibration strategies and to ensure consistency of ambient air measurements (Fig. 1b–c). In the laboratory, three reference gases (Ref1–Ref3) were analyzed for 30 min each, while at the Jurong and SORPES sites, three (WS1–WS3) and two (WS4–WS5) reference gases were measured, respectively. Each field measurement lasted 10 min, and the final 5 min were averaged for analysis. This window was chosen to avoid stabilization effects immediately after valve switching and to represent the stable plateau of each injection. The Allan deviation of $\delta^{13}CH_4$ (raw) decreases monotonically over the accessible τ range, with σ (300 s) = 0.0095 ‰ and σ (600 s) = 0.0048 ‰ (Fig. A2), and no drift-dominated upturn is observed within this range. Although 600 s yields lower random noise, we retain 5-min averaging as a practical compromise that already provides very low short-term noise while improving operational efficiency and reducing the consumption of both reference and working-standard gases. At Jurong, where no drying was applied, reference gases became humidified in the sampling lines; these values were first corrected for H_2O interference before calibration. A detailed description of all reference gases is given in Table 1.

For the assigned reference-gas values (Ref1–3), CH_4 mole fractions were reported on the WMO X2004A scale and $\delta^{13}CH_4$ values were reported relative to the VPDB scale. The remaining working standard gases (WS1–WS5) were assigned in our laboratory by calibration against Ref1–3, thereby tying our working scale to the INSTAAR laboratory scale. The working standard gases were calibrated using the isotopologue-specific approach. Section 2.3 then describes two alternative strategies for applying these assigned values to calibrate and correct the laboratory and field measurements. To assess calibration performance, mid-level references (WS2 at Jurong and Ref2 in the laboratory) were treated as "targets", while the remaining references were used for calibration. Correction coefficients derived from linear interpolation between reference and measured values were then applied to the target periods.

All reference gas values used in this study, across both laboratory and field experiments, were traceable to internationally recognized calibration scales. CH_4 mole fractions were reported on the World Meteorological Organization (WMO) X2004A scale. $\delta^{13}CH_4$ values were reported relative to the Vienna Pee Dee Belemnite (VPDB) scale and were linked through assigned reference-gas values, including manufacturer-certified values for Ref1–Ref3 and laboratory-assigned values for the remaining reference gases using working standards linked to the Institute of Arctic and Alpine Research (INSTAAR, University of Colorado Boulder) laboratory scale. Section 2.3 then describes two alternative strategies for applying these assigned reference-gas values to calibrate and correct the laboratory and field measurements.

2.3 Calibration and correction strategies

Following the water vapor correction, two calibration strategies were applied to derive $\delta^{13}CH_4$ from the analyzer outputs, which were the isotopologue-specific calibration approach (Wen et al., 2013; Griffith, 2018) and the direct $\delta^{13}CH_4$ calibration method (delta-based). These methods were evaluated under both dry and humidified reference gas conditions.

2.3.1 Isotopologue-specific calibration

This method involves two steps: (1) Separate linear correction equations were established for $^{12}CH_4$ and $^{13}CH_4$ using two reference gases with significantly different isotopologue

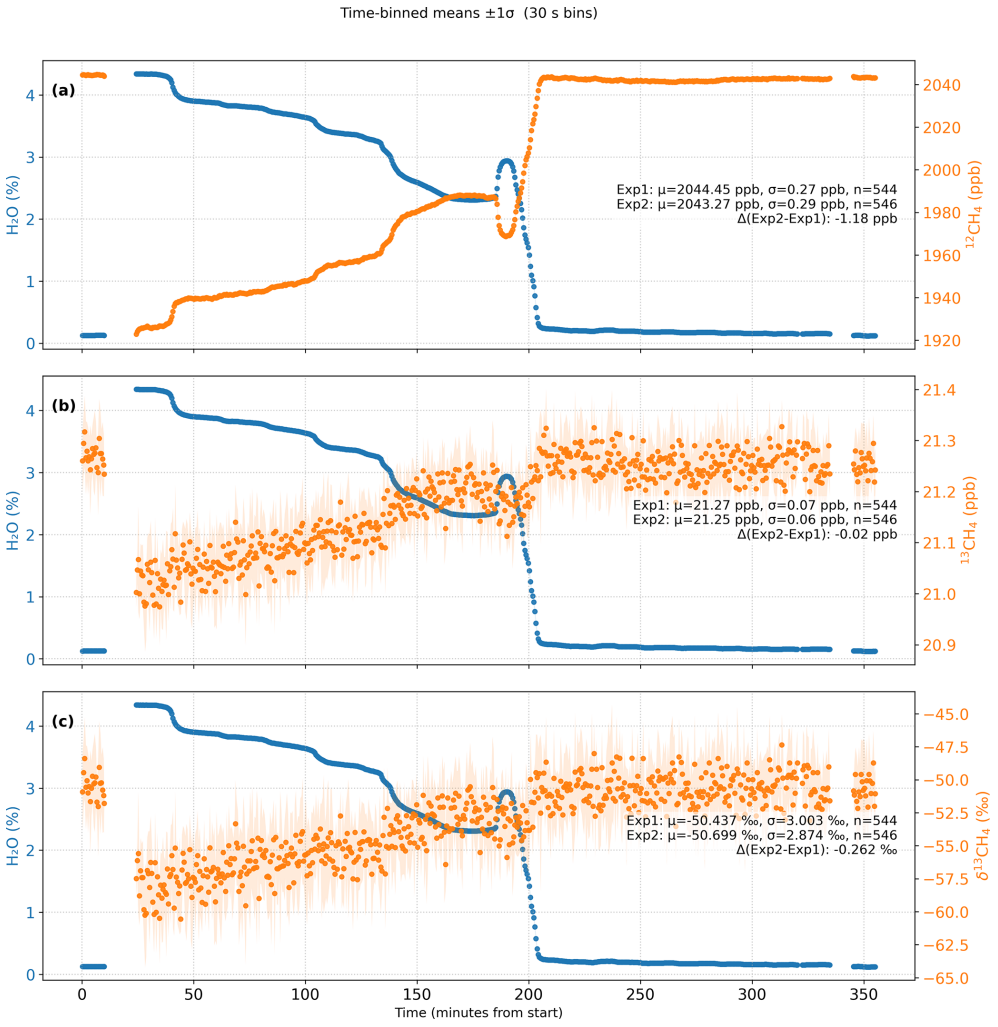

Figure 2. Time series of H_2O, $^{12}CH_4$, $^{13}CH_4$, and $\delta^{13}CH_4$ during the controlled humidity experiment. Each point represents a 30 s mean value, and the shaded areas indicate the 1σ standard deviation of each bin. Exp1 and Exp2 correspond to the dry reference gas measurements performed before and after the artificially humidified period, respectively. The annotated statistics in each panel show the mean (μ), standard deviation (σ), number of averaged points (n), and the drift (ΔExp2–Exp1), demonstrating the measurement stability of $^{12}CH_4$, $^{13}CH_4$, and $\delta^{13}CH_4$ across the humidified period. H_2O represents the water vapor mole fraction (in %).

concentrations. Calibration coefficients a and b were determined from the linear relationship between calibrated and observed values. (2) These coefficients were subsequently applied to the target sample measurements to calculate the total CH_4 concentration and $\delta^{13}CH_4$ values using the following equations:

$$^{12}CH_{4,true} = a_{12} \times {}^{12}CH_{4,dry} + b_{12} \quad (1)$$

$$^{13}CH_{4,true} = a_{13} \times {}^{13}CH_{4,dry} + b_{13} \quad (2)$$

$$\delta^{13}CH_{4,cal} = \frac{{}^{13}r}{{}^{13}r_{ref}} - 1 \quad (3)$$

$$CH_4 = {}^{12}CH_4 \times R_{sum} \quad (4)$$

$${}^{13}r = {}^{13}CH_4/{}^{12}CH_4 \quad (5)$$

$$R_{sum} = \left(1 + {}^{13}r\right)\left(1 + {}^{2}r\right)^4 \quad (6)$$

$${}^{2}r = {}^{2}r_{ref} \times \left(\frac{\delta_D}{1000} + 1\right) = 0.00014018 \quad (7)$$

To perform the correction, the mole fractions of $^{12}CH_4$ and $^{13}CH_4$, as well as the $\delta^{13}CH_4$, and δD-CH_4 values of

Table 1. Certified values of CH_4 molar fraction and $\delta^{13}CH_4$ for dry and humidified reference gases.

Reference					$^{12}CH_4$(ppb)	$^{13}CH_4$ (ppb)
Standard	CH_4 (ppb)	$\delta^{13}CH_4$ (‰)	^{13}r	R_{sum}	True values	
WS1	2004.32 ± 0.57	-46.80 ± 0.035	0.010656929	1.011223724	1982.07 ± 0.564	21.12 ± 0.006
WS2	3592.80 ± 0.3	-47.01 ± 0.035	0.010654656	1.011221449	3552.93 ± 0.297	37.86 ± 0.030
WS3	5017.03 ± 1.5	-47.16 ± 0.021	0.010652979	1.011219770	4961.36 ± 1.48	52.85 ± 0.020
WS4	1985.35 ± 0.11	-48.00 ± 0.700	0.010645125	1.011274904	1963.34 ± 1.1	20.90 ± 0.010
WS5	1983.94 ± 0.07	-49.06 ± 0.700	0.010632171	1.011261942	1961.97 ± 1.1	20.86 ± 0.010
Ref1	1831.6 ± 0.3	-47.85 ± 0.671	0.010645205	1.011211993	1811.29 ± 0.3	19.28 ± 0.014
Ref2	1979.9 ± 0.3	-48.14 ± 0.534	0.01064203	1.011208816	1957.95 ± 0.3	20.84 ± 0.012
Ref3	2219.2 ± 0.3	-45.98 ± 0.497	0.01066609	1.011232889	2194.55 ± 0.3	23.41 ± 0.013

Note: CH_4 and $\delta^{13}CH_4$ are certified values for each standard gas. ^{13}r denotes the ratio between $^{13}CH_4$ and $^{12}CH_4$, calculated from Eq. (5). R_{sum} is the total isotopologue normalising factor for methane, defined in Eq. (6). This correction accounts for the absorption effects introduced by the presence of hydrogen isotopologues such as CH_3D in atmospheric methane, in addition to carbon isotopologues. $^{12}CH_4$ and $^{13}CH_4$ were derived quantities calculated from assigned total CH_4 and $\delta^{13}CH_4$; their uncertainties were obtained by uncertainty propagation. In this cylinder set, WS1–WS5 are working standards calibrated against Ref1–Ref3. Ref1–Ref3 have manufacturer-certified CH_4 and $\delta^{13}CH_4$ values and are used as the reference standards for the calibration of WS1–WS5.

Table 2. Summary of observation settings at the SORPES and Jurong stations.

Site	Environmental Conditions	Target Sample	Selected Period
SORPES	Urban background, low humidity (H_2O: 0.04 %–0.40 %)	From the environment air at 70.0 m	DOY240–280 in 2022
Jurong	Rice paddy, high humidity (H_2O: 0.93 %–3.5 %)	From rice canopy at 3.0 m	DOY 240–280 in 2018

each reference gas, must be known. Here, $^{12}CH_4$ and $^{13}CH_4$ represent the measured mole fractions (ppb) of the two carbon isotopologues of CH_4, obtained directly from the spectrometer under dry air conditions. CH_4 in Eq. (4) denotes the total methane mole fraction, i.e., the sum of all isotopologues. $\delta^{13}CH_4$ (‰, VPDB scale) and δD–CH_4 (‰, Vienna Standard Mean Ocean Water, VSMOW scale) denote the carbon and hydrogen isotopic compositions of methane, with values reported in per mil (‰), respectively, determined based on certified reference gases or previous intercomparison results. Constants used in the calculations included $^{13}r_{ref} = 0.0111802$ (VPDB) and $^{2}r_{ref} = 0.00015575$ (VSMOW), which are the internationally accepted reference isotope ratios for ^{13}C / ^{12}C and D/H, respectively, as recommended by Werner and Brand (2001).

The parameters a_{12}, b_{12}, a_{13}, and b_{13} represent the slope and intercept of the calibration equations for $^{12}CH_4$ and $^{13}CH_4$, respectively. They correct the instrument response and convert the raw isotopologue signals into calibrated mole fractions. For field processing, these coefficients were linearly interpolated in time between calibration periods, rather than applying an interval-mean approximation, to obtain time-resolved calibration parameters for each measurement. The isotope ratio ^{13}r is calculated directly from the calibrated isotopologue mole fractions, and the total isotopologue normalization factor R_{sum} accounts for all possible isotopic substitutions in CH_4, including hydrogen-bearing species such as CH_3D, following Griffith (2018). An assumed δD value of -100 ‰ for atmospheric CH_4 was adopted from Quay et al. (1999). All calibrated values were reported on the WMO X2004A scale, and all isotopic ratios are reported relative to the VPDB (for $\delta^{13}CH_4$) and VSMOW (for δD) international reference scales.

A sensitivity estimate was conducted to assess the impact of uncertainty in the assumed atmospheric δD–CH_4 on R_{sum} and total CH_4 mole fraction. Taking δD–$CH_4 = -100$ ‰ as a representative value, a conservative ± 50 % variation (-50 ‰ to -150 ‰) changes ^{2}r by ± 5.6 %, but propagates to R_{sum} in Eq. (6) at only ± 0.0031 %. This corresponds to < 0.1 ppb uncertainty in total CH_4 for typical atmospheric mole fractions of 2000–3000 ppb, which is negligible relative to measurement uncertainty. Note that R_{sum} is used only to convert $^{12}CH_4$ to total CH_4 and does not enter the calculation of $\delta^{13}CH_4$, which is determined from the ratio $^{13}CH_4/^{12}CH_4$.

In this study, all humidity-correction functions were derived from the raw (uncorrected) outputs, and all subsequent analyses were performed using the raw $^{12}CH_4$, $^{13}CH_4$, and $\delta^{13}CH_4$ values with the offline empirical humidity correction developed here. The manufacturer-corrected outputs were not used in the calibration workflow to avoid double correction.

2.3.2 Delta-based calibration

The delta-based calibration approach corrects instrumental drift using $\delta^{13}CH_4$ directly. A linear calibration is established using two reference gases with distinct $\delta^{13}CH_4$ signatures as Eq. (8):

$$\delta^{13}CH_{4,cal} = a_\delta \times \delta^{13}CH_{4,dry} + b_\delta \quad (8)$$

Here, a_δ and b_δ represent the slope and intercept of the delta-based calibration, respectively, which account for small systematic differences between the spectrometer-derived $\delta^{13}CH_4$ values and the true isotopic compositions of the reference gases. In both field measurements, the two reference gases used for the delta-based calibration had very similar $\delta^{13}CH_4$ values. Therefore, a_δ was effectively set to 1 and the delta-based calibration was implemented as a one-point correction. These coefficients correct residual scale offsets and sensitivity deviations in the $\delta^{13}CH_4$ retrievals before converting all measurements to the VPDB scale. This calibration is then applied to field observations, and $\delta^{13}CH_4$ values are reported on the VPDB scale.

2.4 Correlation and statistics analysis

All statistical analyses were performed with a significance threshold of $p < 0.05$. Uncertainties were expressed as 95 % confidence intervals derived from bootstrap resampling. To assess the error characteristics, residuals and inter-method differences were visualized as histograms and fitted with Gaussian functions. The mean, standard deviation (σ), RMSE, and MAE were computed to characterize the residual statistics. Gaussian functions were fitted to the histograms to examine whether the residuals followed a normal distribution.

3 Results and Discussion

3.1 Water vapor correction functions

We first performed laboratory experiments to quantify the water vapor effect on isotopologue mole fractions and $\delta^{13}CH_4$. Reference gases with known CH_4 mole fractions and $\delta^{13}CH_4$ values were humidified to obtain varying H_2O levels. The experiments revealed systematic dependencies of the $^{12}CH_4$ and $^{13}CH_4$ mole fractions and $\delta^{13}CH_4$, on H_2O concentrations (Fig. 3a–c).

From these measurements, we established quadratic polynomial correction functions to describe the H_2O dependence of isotopologue mole fractions (Eqs. 9–10), and derived an empirical linear function for $\delta^{13}CH_4$ (Eq. 11). These relationships form the foundation for the water correction in field evaluations of calibration strategies (Sect. 3.3).

$$\frac{^{12}CH_{4,wet}}{^{12}CH_{4,dry}} = 1 - 0.0103 \times H_2O - 6.96 \times 10^{-4} \times (H_2O)^2 \quad (9)$$

$$\frac{^{13}CH_{4,wet}}{^{13}CH_{4,dry}} = 1 - 6.29 \times 10^{-4} \times H_2O - 3.94 \times 10^{-4} \times (H_2O)^2 \quad (10)$$

$$\delta^{13}CH_{4,\,dry} = \delta^{13}CH_{4,\,wet} - 1.36 \times H_2O \quad (11)$$

Here, the "wet" mole fractions represent values observed from the humidified reference gas in laboratory conditions, while the "dry" values correspond to the instrument-measured dry baseline. The baseline was obtained from the low-humidity segment at the end of the experiment ($H_2O < 0.13$ %). H_2O denotes the water vapor concentration (%) directly measured by the analyzer (column "H_2O"). For Eq. (9), the quadratic fit for $^{12}CH_4$ is robust ($R^2 \approx 1.000$), with fitted uncertainties of $\pm 1.2 \times 10^{-4}$ for the linear term and $\pm 3.9 \times 10^{-5}$ for the quadratic term. For Eq. (10), the quadratic dependence for $^{13}CH_4$ is also significant ($R^2 \approx 0.912$), and the fitted uncertainties are $\pm 3.8 \times 10^{-4}$ and $\pm 1.2 \times 10^{-4}$ for the linear and quadratic terms, respectively. For Eq. (11), $\delta^{13}CH_{4,\,wet}$ exhibits a linear dependence on water vapor concentration, deviating from the dry reference $\delta^{13}CH_{4,\,dry}$ by -1.36 ± 0.10 ‰ per % H_2O ($R^2 \approx 0.839$).

The residual statistics of the fitted water vapor correction functions are shown in Fig. 3d–f, and detailed summarized in Table 3. The absolute residuals between the binned means and the fitted values were mostly small, confirming that the empirical corrections effectively capture the water vapor dependencies within 0.15 %–4.0 % H_2O. For $^{12}CH_4$, 80 % of the absolute residuals were below 0.93 ppb and 90 % below 1.09 ppb, corresponding to less than 0.05 % of the $^{12}CH_4$ reference concentration. The $^{13}CH_4$ residuals were similarly low, with 80 % and 90 % below 0.033 and 0.041 ppb (median = 0.021 ppb, RMS = 0.029 ppb). For $\delta^{13}CH_4$, the median and 80th percentile residuals were 0.63 ‰ and 1.68 ‰, respectively. Both $^{12}CH_4$ and $^{13}CH_4$ required quadratic correction functions to accurately describe the nonlinear response to water vapor, reflecting the combined influence of dilution and pressure-broadening effects on observed absorption peak heights. This nonlinear behavior is consistent with previous characterizations of CRDS instruments (Chen et al., 2010; Wen et al., 2013; Griffith, 2018).

For $^{12}CH_4$, the fitted coefficients (-0.0103 for the linear and -6.96×10^4 for the quadratic term) closely match those reported by Chen et al. (2010) for bulk CH_4, confirming the reproducibility of the water vapor interference across different analyzer models and laboratory setups. For $^{13}CH_4$, the same quadratic correction was applied. Although the absolute residuals are small (80th percentile = 0.033 ppb), the fractional deviation is larger than for $^{12}CH_4$ because the $^{13}CH_4$ dry mole fraction is only ~ 21 ppb. Quantitatively, the 80th percentile residual corresponds to a relative uncer-

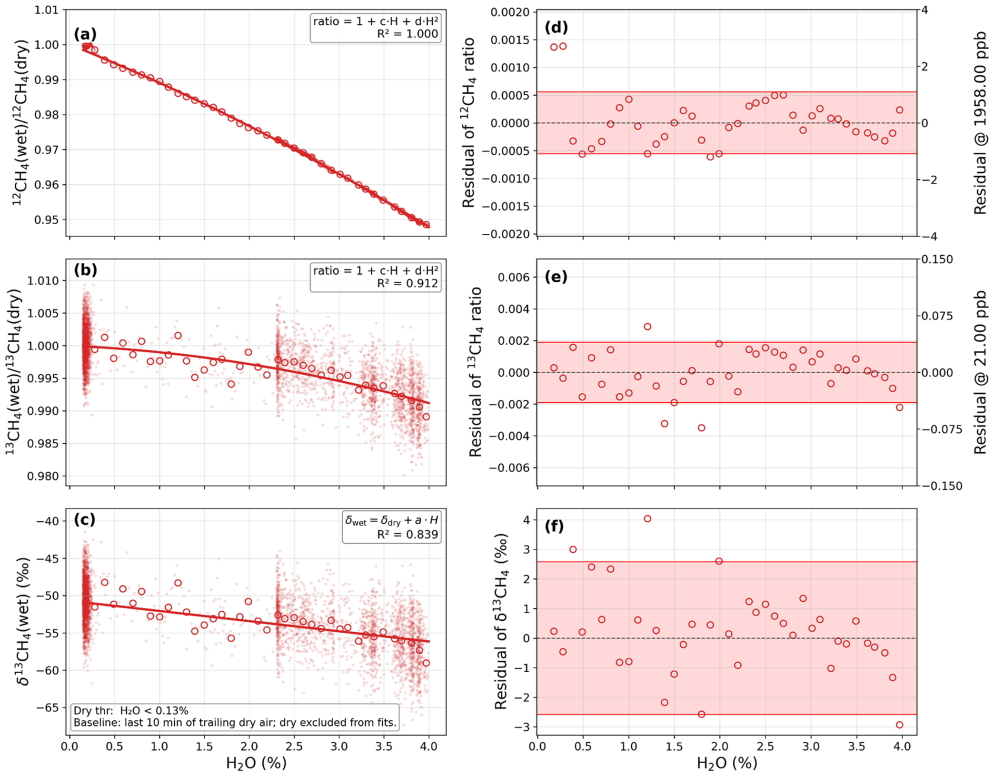

Figure 3. Water vapor correction functions for $^{12}CH_4$, $^{13}CH_4$, and $\delta^{13}CH_4$ derived from laboratory water vapor experiments (0.15 %–4.0 % H_2O). Panels **(a)**, **(b)**, and **(c)** show the fitted relationships between H_2O concentration and the wet-to-dry ratios of $^{12}CH_4$, the wet-to-dry ratios of $^{13}CH_4$, and the $\delta^{13}CH_4$ deviation ($\delta^{13}CH_{4,\,wet} - \delta^{13}CH_{4,\,dry}$), respectively. Each open circle represents the mean value within a 0.1 % H_2O bin. The solid red lines indicate the best-fit regression models (quadratic for $^{12}CH_4$ and $^{13}CH_4$, linear for $\delta^{13}CH_4$), and small points indicate raw observations. Panels **(d)**, **(e)**, and **(f)** show the corresponding residuals; the red shaded bands indicate the interval containing 90 % of the data points, with parameters detailed in Table 3.

Table 3. Summary statistics of water vapor correction residuals for $^{12}CH_4$, $^{13}CH_4$, and $\delta^{13}CH_4$.

Parameter	Baseline	Min	Median	80th percentile	90th percentile	Max	RMS
$^{12}CH_4$	1957.95 ppb	0.0034	0.5022	0.9346	1.0921	2.7090	0.8577
$^{13}CH_4$	20.84 ppb	0.0019	0.0213	0.0325	0.0413	0.0734	0.0288
$\delta^{13}CH_4$	−48.14 ‰	0.0970	0.6297	1.6761	2.5786	4.0386	1.4215

Residuals were calculated as the absolute difference between binned means and fitted values from the water vapor correction functions for the experiment (0.15 %–4.0 % H_2O). Reported statistics include minimum (Min), median, 80th and 90th percentile (80th percentile and 90th percentile), maximum (Max), and Root Mean Square (RMS) residuals. Percentile metrics (P80, P90) are used to represent the typical residual range while minimizing the influence of a few extreme humid points. All values are absolute residuals; $^{12}CH_4$ and $^{13}CH_4$ are in ppb, and $\delta^{13}CH_4$ in ‰.

tainty of approximately 0.15 % for $^{13}CH_4$, compared with ∼ 0.05 % for $^{12}CH_4$, indicating that the $^{13}CH_4$ channel has about three times higher relative uncertainty. This suggests that the $^{13}CH_4$ signal is intrinsically more vulnerable to residual water bias. Because $\delta^{13}CH_4$ is derived from the ratio of $^{13}CH_4$ to $^{12}CH_4$, any remaining humidity-dependent bias in $^{13}CH_4$ directly propagates into $\delta^{13}CH_4$. In practice, this means that the accuracy of the isotopologue-specific calibration strategy under humid conditions is ultimately limited by the performance of the $^{13}CH_4$ water vapor correction.

By contrast, $\delta^{13}CH_4$ exhibited an approximately linear dependence on water vapor. This behavior arises because the nonlinear contributions in the numerator and denominator largely cancel when expressed as a ratio, leaving a dominant first-order term. This partial cancellation of nonlinear terms reflects the mathematical structure of $\delta^{13}CH_4$ as a ratio, where similar H_2O dependencies in $^{12}CH_4$ and $^{13}CH_4$ tend to offset each other. Although the $\delta^{13}CH_4$-H_2O regression shows larger scatter than those for the individual isotopologues, the fitted slope of -1.36 ± 0.10 ‰ %$^{-1}$, H_2O over

the full experimental range of 0.15–4.0 % H_2O reflects enhanced sensitivity at higher humidity levels. When restricted to the same water vapor interval (≤1.5 %), our fitted slope of -1.00 ± 0.52 ‰ $\%^{-1}$ H_2O is not significantly different from the reported slope of -0.54 ± 0.29 ‰ $\%^{-1}$ H_2O by Hoheisel et al. (2019).

It is worth noting that physical drying to approximately 0.1 % H_2O remains the recommended best practice for achieving sub-per-mil $\delta^{13}CH_4$ accuracy (e.g., Rella et al., 2015). In our study, the empirical water vapor correction functions were derived for the H_2O range of 0.15 %–4.0 %, which provide a complementary solution for measurements in humid air.

3.2 Comparison of $\delta^{13}CH_4$ calibration strategies for dry air sample measurements

For dry air sample measurements, both the isotopologue-specific and the delta-based calibration strategies yielded consistent $\delta^{13}CH_4$ results, with small and relatively stable offsets. For the certified target gas (Fig. 4), both calibrated values were close to the assigned reference, with mean residuals of 0.15 ‰ for the isotopologue-specific method and 0.55 ‰ for the delta-based method. The inter-method difference ($\Delta\delta^{13}CH_4$ = iso – delta) averaged −0.40 ‰, indicating a slight but systematic offset toward lighter $\delta^{13}C$ in the delta-based calibration. Residuals and differences followed approximately normal distributions, and their root-mean-square and mean absolute errors were both close to 2 ‰, comparable to the typical instrumental precision of the analyzer.

For measurements of air samples dried with the Nafion™ membrane dryer at the SORPES station (Fig. 5), both calibration schemes showed highly consistent $\delta^{13}CH_4$ retrievals. The two approaches yielded overlapping daily means throughout DOY 240–280, with differences mostly within the 1σ range of observational variability. The inter-method difference ($\Delta\delta^{13}CH_4$) averaged 0.29 ‰ and exhibited a near-Gaussian distribution ($\sigma = 0.71$ ‰), indicating minimal systematic bias between the two schemes for dried air sample measurements. A significant correlation between $\Delta\delta^{13}CH_4$ and CH_4 mole fraction ($R^2 = 0.97$, $p < 0.001$) suggests that part of the residual offset may result from concentration-dependent effects of delta-based calibration. Although the ambient data showed slightly higher variability than laboratory measurements, both calibration methods remained stable and consistent across a wide range of CH_4 concentrations, demonstrating reliable performance for dried-air applications.

For dry air sample measurements, both calibration strategies yielded nearly identical $\delta^{13}CH_4$ results, indicating that the isotopic retrievals are consistent when water vapor interference is negligible. However, a strong correlation between the inter-method difference ($\Delta\delta^{13}CH_4$) and CH_4 mole fraction (Fig. 5b) suggests that concentration-dependent effects may still influence the delta-based calibration. The $\Delta\delta^{13}CH_4$ exhibits a clear and consistent dependence on CH_4 mole fraction across the three concentration subsets (Fig. A2a–c). Examination of the two retrievals separately further indicates that both calibration formulations vary with CH_4 mole fraction, but with different magnitudes and response patterns (Fig. A2d–f). The isotopologue-specific calibrated $\delta^{13}CH_4$ shows a clearer CH_4 dependence in all subsets (Fig. A2g–i), whereas the delta-based retrieval also varies with CH_4 but generally with weaker explanatory power (lower R^2) and a different slope structure (Fig. A2g–i). Thus, the concentration dependence of $\Delta\delta^{13}CH_4$ reflects the different concentration sensitivities of the two calibration strategies and their combined propagation into the inter-method difference.

Although the present dataset cannot explicitly isolate the cause, this pattern agrees well with the theoretical framework of Griffith et al. (2012), which demonstrated that non-zero intercepts and nonlinearities in isotopologue calibrations inevitably propagate into $\delta^{13}C$ space, producing apparent $\delta^{13}C$-concentration coupling. Griffith (2018) further generalized this analysis, identifying both inverse and linear dependencies of $\delta^{13}CH_4$ on CH_4 concentration. Our results exhibit the concentration-dependent behavior predicted by these studies. Similar dependencies have also been reported for CO_2 isotope measurements (Wen et al., 2013; Pang et al., 2016; Braden-Behrens et al., 2017), indicating that such effects are intrinsic to $\delta^{13}C$-based formulations rather than instrument-specific anomalies. Beyond the dry air regime examined here, additional deviations may emerge in humid air, where spectral interference becomes a dominant factor influencing isotopic accuracy.

The concentration dependence diagnosed here suggests that, in future deployments, CH_4 concentration dependence could be incorporated directly into the delta-based calibration. With a set of at least 3 reference gases covering a reasonable CH_4 concentration range, the linear delta-based calibration (Eq. 8) could be replaced with a 3-parameter equation presented in Eq. (15) of Griffith (2018), without requiring a spread in $\delta^{13}CH_4$ values across the reference gases. To further assess the robustness of these correction functions under realistic environmental conditions, we examined their performance in humidified air samples at the rice paddy site.

3.3 Performance of calibration strategies under humid air conditions

To evaluate the performance of the water vapor correction under field conditions, both calibration strategies were applied to a humidified target gas at the rice paddy site (DOY 240–280, 2018). As shown in Fig. 6, after applying the correction functions, both isotopologue-specific and delta-based calibrations reproduced $\delta^{13}CH_4$ values close to the certified reference (Fig. 6a), confirming that the equations effectively removed humidity-induced artifacts. The isotopologue-specific calibration yields $\delta^{13}CH_4$ values that align more tightly with the reference, while the delta-based

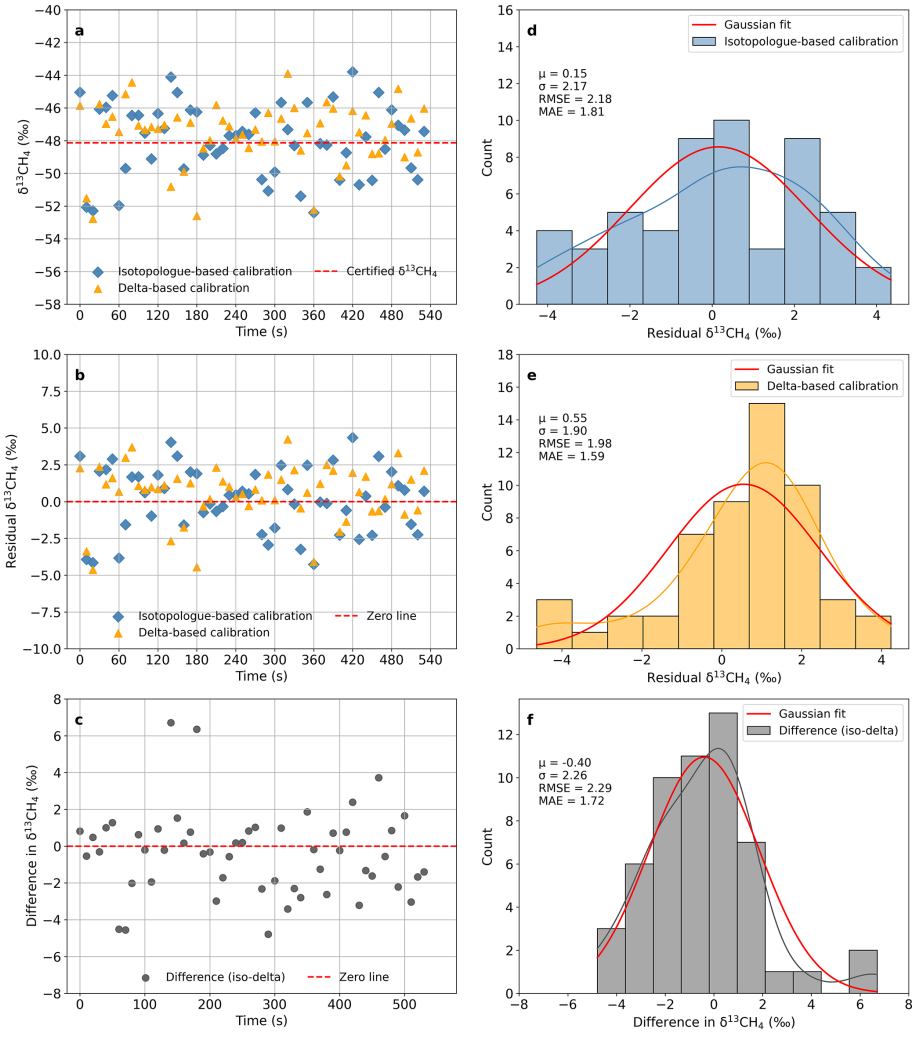

Figure 4. Comparison of $\delta^{13}CH_4$ calibration strategies for a dry reference gas. **(a)** Calibrated $\delta^{13}CH_4$ from isotopologue-specific (blue diamonds) and delta-based (yellow triangles) strategies; the reference is shown as a red dashed line. **(b)** Residuals (calibrated – certified) for both strategies. **(c)** Time series of the difference between isotopologue-specific and delta-based calibrated $\delta^{13}CH_4$ (hereafter referred to as the inter-method difference, iso – delta). **(d, e)** Histograms of residuals for the two strategies with Gaussian fits. **(f)** Distribution of the inter-method difference (iso – delta) with a Gaussian fit. For **(d)**–**(f)**, Gaussian fits provide the mean (μ) and standard deviation (σ), while root-mean-square error (RMSE) and mean absolute error (MAE) are computed from the data. All results are based on 10-s averaged data.

calibrated results retain a small positive offset (Fig. 6a–c). Consistent with the histograms, the isotopologue-specific residuals improved from $\mu = -0.84\,‰$ ($\sigma = 0.30\,‰$) before correction to $\mu = -0.31\,‰$ ($\sigma = 0.24\,‰$) after correction. In contrast, the delta-based residuals remained consistently near $+0.5\,‰$ both before and after correction ($\mu \approx +0.48$ to $+0.49\,‰$, $\sigma = 0.26\,‰$; Fig. 6d–e). The inter-method difference (iso – delta) has a mean of $-0.80\,‰$ after correction with a reduced spread ($\sigma = 0.14\,‰$; Fig. 6f), indicating a stable, strategy-dependent offset. These results confirm that the correction equations effectively mitigate humidity-induced artifacts, particularly for the isotopologue-specific approach, providing a reliable basis for subsequent field validation.

The Jurong site represents a typical rice paddy ecosystem, characterized by persistently high ambient humidity and strong methane emissions. During the observation period, H_2O concentrations frequently exceeded 3 %, while CH_4 mole fractions varied substantially, ranging from background levels below 2000 ppb to episodic peaks above 5000 ppb. These conditions provide a stringent test for calibration strategies, as both elevated humidity and broad concentration ranges can amplify systematic biases in $\delta^{13}CH_4$ retrievals.

Figure 7 illustrates the contrasting behavior of isotopologue-specific and delta-based calibrations for humid air observations. Daily mean $\delta^{13}CH_4$ values from the delta-based calibration were consistently offset relative to those from the isotopologue-specific approach, and exhibit

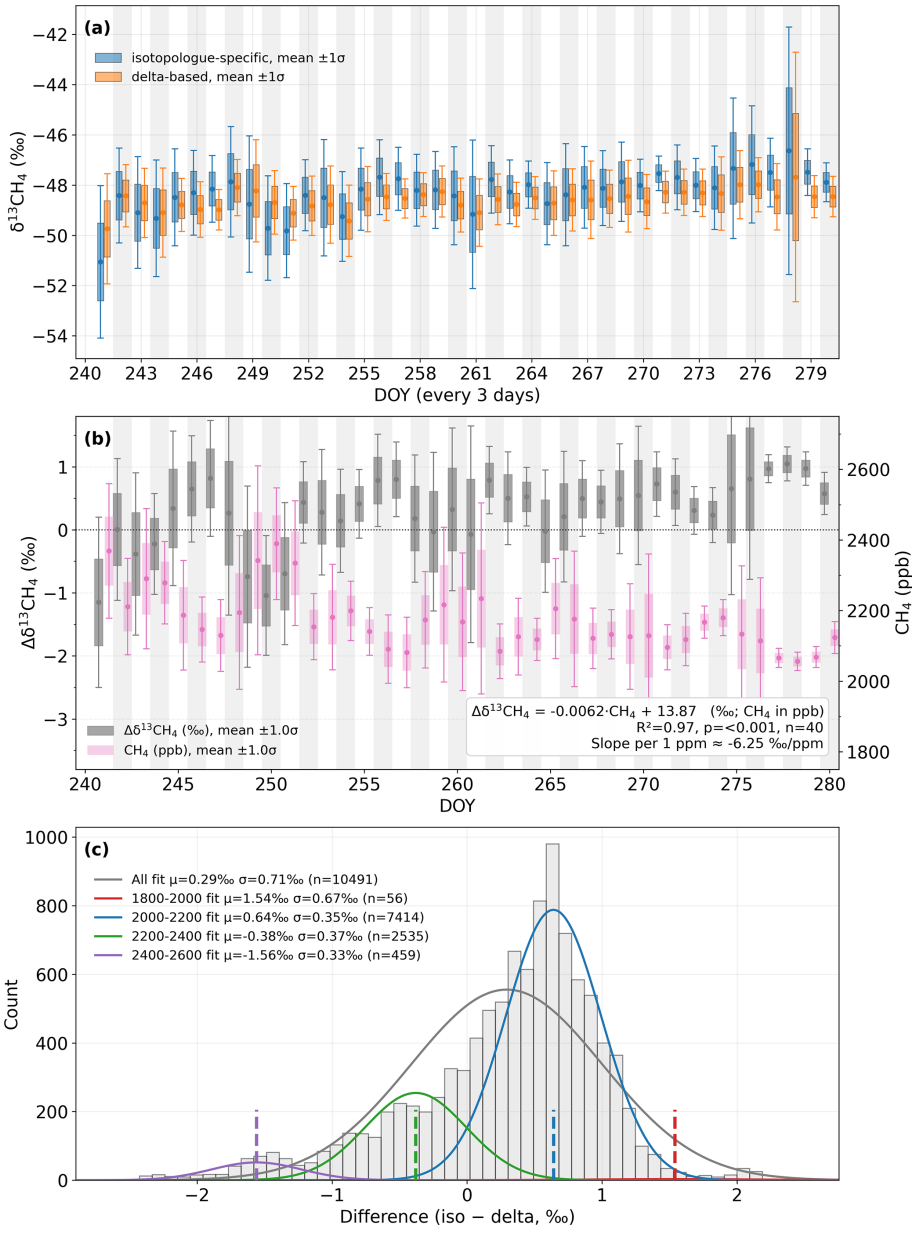

Figure 5. Comparison of $\delta^{13}CH_4$ calibration strategies at the SORPES station (dried ambient air, DOY 240–280, 2022). **(a)** Daily averaged $\delta^{13}CH_4$ values from isotopologue-specific (blue) and delta-based (orange) calibration strategies, with 1σ standard deviations. **(b)** Time series of the inter-method difference $\Delta\delta^{13}CH_4$ (iso – delta, grey bars) and corresponding CH_4 mole fraction (pink bars, right axis). The linear relationship between $\Delta\delta^{13}CH_4$ and CH_4 is shown with a fitted regression. **(c)** Histogram of $\Delta\delta^{13}CH_4$ (iso − delta) for all data and for different CH_4 concentration ranges, each fitted with a Gaussian function. The fitted mean (μ) and standard deviation (σ) are reported for each subset. All analyses are based on 5-min averaged data.

greater variability (Fig. 7a). The inter-method difference, $\Delta\delta^{13}CH_4$ (iso − delta), closely tracked temporal variations in both H_2O and CH_4 mole fractions (Fig. 7b), exhibiting significant correlations with H_2O ($R^2 = 0.91$, $p < 0.001$) and with CH_4 ($R^2 = 0.28$, $p < 0.001$). The overall $\Delta\delta^{13}CH_4$ distribution is centered at $-1.06\,‰$ ($\sigma = 1.92\,‰$; $n = 3126$) (Fig. 7c). This bias varies with CH_4 concentration, and the fitted mean $\Delta\delta^{13}CH_4$ shifts from $-1.55\,‰$ (2000–2500 ppb) to $+2.20\,‰$ (5000–5500 ppb) (Fig. 7c).

To further interpret Fig. 7, we added the Jurong correlation analysis in Fig. A1. The inter-method difference ($\Delta\delta^{13}CH_4$) shows only a weak relationship with CH_4 mole fraction ($R^2 \approx 0.30$) and is not statistically significant ($p > 0.05$; Fig. A1a), which may reflect the intrinsic concentration depen-

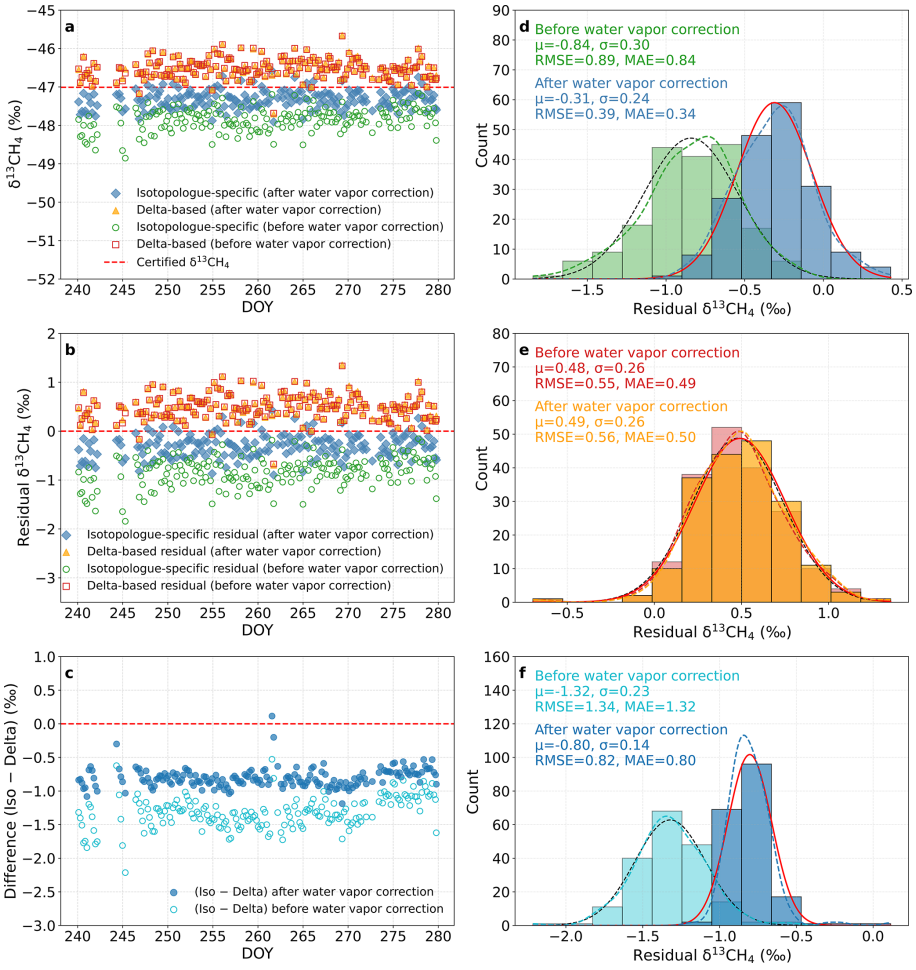

Figure 6. Comparison of $\delta^{13}CH_4$ calibration strategies for a humidified target gas (rice paddy site, DOY 240–280, 2018). **(a)** $\delta^{13}CH_4$ values from the isotopologue-specific (blue diamonds) and delta-based (orange triangles) calibrations, shown both before (open symbols) and after (filled symbols) applying the water vapor correction. The certified reference value is indicated by the red dashed line. **(b)** Residuals (calibrated – certified) for both calibration strategies, with open and filled markers representing results before and after water vapor correction, respectively. **(c)** Time series of the inter-method difference $\Delta\delta^{13}CH_4$ = (iso – delta), shown before (open) and after (filled) water vapor correction. **(d, e)** Histograms of residuals for the two calibration strategies before and after water vapor correction, with Gaussian fits illustrating their respective distributions. **(f)** Histogram of the inter-method difference (iso − delta) before and after water vapor correction, also fitted with Gaussian functions. For panels **(d)**–**(f)**, Gaussian fits provide the mean (μ) and standard deviation (σ), while the root-mean-square error (RMSE) and mean absolute error (MAE) are calculated from the data. All results are based on 5-min averaged measurements after applying the empirical water vapor correction equations functions.

dence for the delta-based approach has been reported previously (Rella et al., 2015; Miles et al., 2018).

In contrast, $\Delta\delta^{13}CH_4$ correlates strongly with H_2O ($R^2 \approx 0.91$, $p < 0.001$; Fig. A1b). This is most likely driven by the significant correlation between the calibrated $\delta^{13}CH_4$ using the delta-based approach and H_2O (Fig. A1d), as the correlation between the calibrated $\delta^{13}CH_4$ using the isotopologue-specific approach and H_2O is insignificant (Fig. A1c).

These results highlight that high humidity and large CH_4 variability exacerbate the intrinsic weaknesses of delta-based calibration, consistent with earlier observations for CO_2 isotopes (Wen et al., 2013; Pang et al., 2016). Without explicit correction, such biases can propagate into source signature retrievals, leading to systematic offsets in rice-paddy plume analyses. Although a significant correlation between $\Delta\delta^{13}CH_4$ and H_2O was observed, this may not directly represent a spectroscopic effect of water vapor. At the Jurong site, episodes of high humidity often coincided with strong CH_4 emissions, producing an intrinsic covariance between H_2O and CH_4. Consequently, part of the apparent $\Delta\delta^{13}CH_4$–H_2O relationship may arise from this covariation rather than from water vapor interference alone. The empirical correction functions used here effectively capture the dominant humidity effects at the isotopologue level,

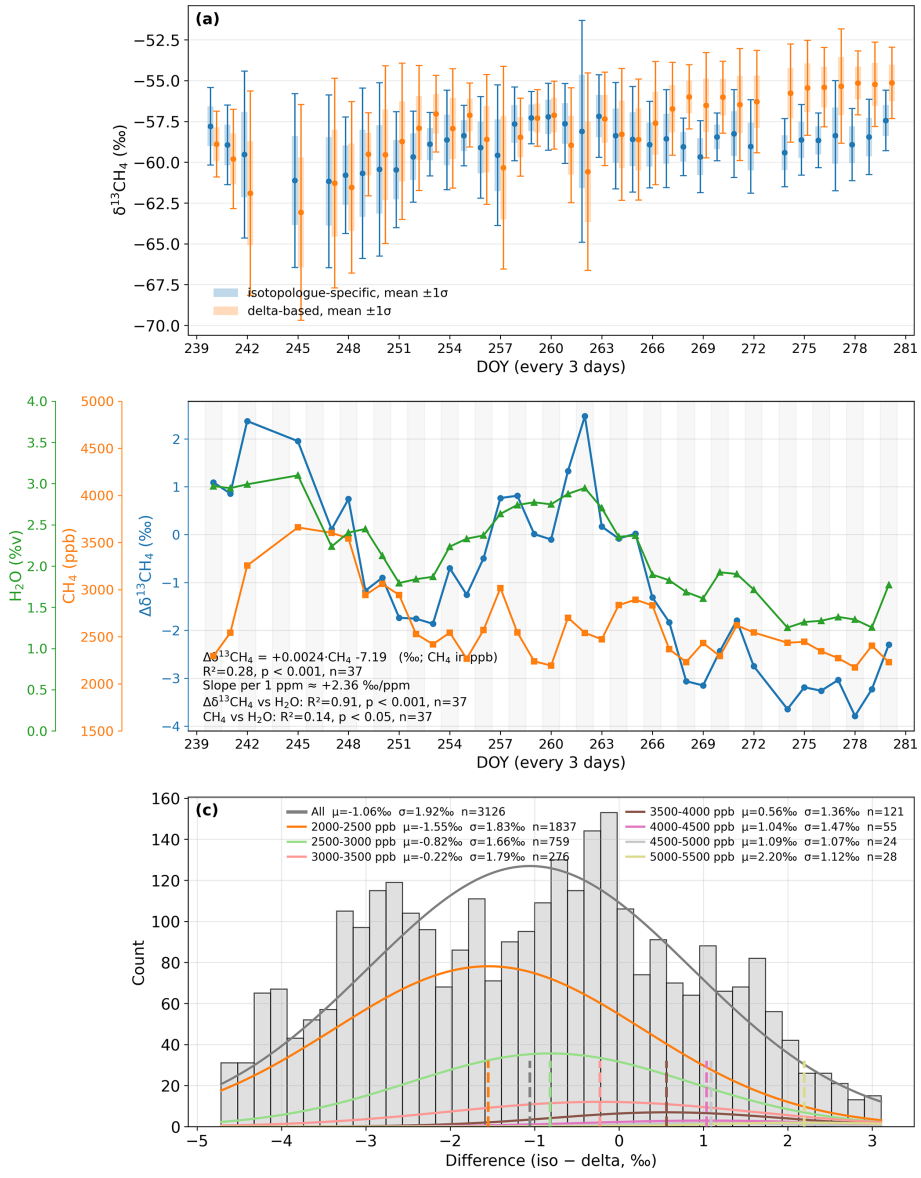

Figure 7. Field comparison of $\delta^{13}CH_4$ calibration strategies for humid air observations at the rice paddy site (DOY 240–280, 2018). **(a)** Daily mean $\delta^{13}CH_4$ from isotopologue-specific (blue) and delta-based (orange) calibrations (mean $\pm 1\sigma$). **(b)** Time series of the inter-method difference in $\delta^{13}CH_4$ (iso – delta, blue line) together with total CH_4 mole fraction (orange line) and H_2O concentration (green line, 0.93 % to 3.5 %). **(c)** Histogram of $\delta^{13}CH_4$ differences (iso – delta) grouped by CH_4 mole-fraction ranges, each fitted with a Gaussian function. The fitted mean (μ) and standard deviation (σ) are reported for each subset. All results are based on 5-min averages.

but may not fully account for additional spectral interferences associated with pressure or temperature variability. After accounting for the H_2O–CH_4 covariance, the remaining concentration dependence is most consistent with intrinsic CH_4 non-linearity reported for CRDS isotope measurements (e.g., Rella et al., 2015; Miles et al., 2018), while residual pressure/temperature-related spectral effects and limitations of empirical corrections may also contribute. We therefore interpret the field results as a combination of effectively corrected first-order humidity effects and residual concentration-dependent behavior that is instrument- and condition-dependent. It should also be emphasized that, in practice, physical drying of air samples remains the preferred approach, whereas empirical water vapor corrections should serve only as a secondary option when drying is not feasible. Addressing these aspects in future work will further refine calibration strategies and enhance their applicability across diverse environments.

3.4 Application of calibration strategies in field observations

Jurong is situated in rice paddy fields and is therefore best characterized as a large-signal, source-influenced environment, and we refer to the WMO/GAW extended compatibility target of ±0.2 ‰ for the target accuracy of our measurements (IAEA, 2024). In contrast, SORPES captures both well-mixed background periods and large-signal episodes, so the appropriate accuracy requirement depends on the specific application and is expected to fall between the WMO/GAW network target (±0.02 ‰, for well-mixed background air) and the extended target (±0.2 ‰, for large-signal (source-influenced/urban) conditions). Our target-gas tests suggest that the isotopologue-specific approach can satisfy the ±0.2 ‰ criterion under dry conditions, and that applying an effective water-vapor correction brings performance close to this extended target under humid conditions. However, in both cases, they do not meet the stringent ±0.02 ‰ compatibility level required for background-network applications. Achieving that level will likely require improved instrumental precision and stability, together with sufficiently frequent calibration to reference gases.

To further quantify the relationship between the inter-method bias ($\Delta\delta^{13}CH_4$) and CH_4 concentration, we regressed $\Delta\delta^{13}CH_4$ against CH_4 mole fraction using the expression $\Delta\delta^{13}CH_4 = c0 + c1/CH_4 + c2 \times CH_4$ following Griffith et al. (2018) (Table 4). At both field sites, most data points are concentrated within a relatively narrow CH_4 range, representing the dominant concentration regimes during field observations: 2000–3000 ppb at Jurong and 2000–2500 ppb at SORPES. These ranges capture the typical operational conditions under which calibration biases are most relevant.

At the Jurong site, $\Delta\delta^{13}CH_4$ exhibited a pronounced $1/CH_4$ dependence, with significantly negative $c1$ terms ($p < 0.01$) and negligible $c2$ values. This pattern indicates that the inter-method difference increases toward lower CH_4 concentrations, where signal dilution and pressure-broadening effects become more influential. Although the water vapor correction successfully mitigates first-order humidity effects, the remaining dependence likely arises from the coupled response of isotopologue scaling and dilution to varying CH_4 and H_2O levels. At the SORPES site, $\Delta\delta^{13}CH_4$ was better characterized by the CH_4 ($c2$) term, showing a weak but positive dependence on concentration ($c2 > 0$, $p < 0.05$). In the absence of strong humidity effects, the difference between isotopologue-specific and delta-based calibrations thus reflects higher-order nonlinearities intrinsic to the delta-based formulation. The contrasting dominant terms between Jurong and SORPES highlight how humidity modulates the expression of calibration nonlinearity: humid air amplifies inverse ($1/CH_4$) dependencies, whereas dry air emphasizes minor linear (CH_4) effects.

These site-specific regressions are consistent with the theoretical framework proposed by Griffith (2018), where the inverse ($1/CH_4$) and linear (CH_4) terms correspond to intercept-driven and quadratic nonlinearities, respectively. The slope variations observed in Fig. 7c further support this interpretation, providing a mechanistic explanation for the site-dependent discrepancies in Figs. 6–7. However, despite the effectiveness of the water vapor correction functions across the full humidity range, the residual concentration dependence of $\Delta\delta^{13}CH_4$ suggests that both CH_4 and H_2O jointly modulate the inter-method bias, with their relative contributions differing between humid and dry air. In practice, field measurements typically include an air-drying stage (e.g., Nafion™ membrane dryers), but physical drying alone cannot fully remove water vapor interference. Even well-maintained Nafion™ systems leave residual H_2O at 0.3 %–0.6 % under ambient conditions – enough to bias $\delta^{13}CH_4$ retrievals, particularly at humid sites or during high-CH_4 events. Therefore, an explicit H_2O correction remains necessary rather than assuming that drying alone ensures isotopic accuracy (Welp et al., 2013; Paul et al., 2020).

Overall, these site-specific behaviors provide practical guidance for field deployment. Under well-dried conditions with relatively stable CH_4 mole fractions (e.g., SORPES), the residual difference between the isotopologue-specific and delta-based calibrations is small, dominated by weak high-concentration nonlinearities, and can be characterized empirically. In such cases, the delta-based approach remains operationally acceptable for routine monitoring. By contrast, for humid air, lower CH_4 conditions with large CH_4 variability (e.g., Jurong), the inter-method bias exhibits a strong inverse-concentration dependence and should not be treated as a constant offset. In these environments, the isotopologue-specific calibration is required to avoid systematic shifts in inferred source signatures. In practice, physical drying of the sample air should remain the primary strategy wherever feasible, and the combination of humidity correction and isotopologue-specific calibration should be considered the default fallback when effective drying cannot be maintained.

4 Conclusions

We evaluated two calibration strategies for $\delta^{13}CH_4$, delta-based and isotopologue-specific calibration, using a Picarro G2201-i isotopic analyzer under both laboratory and field conditions. Empirical water vapor correction functions were established based on laboratory experiments (0.15 %–4.0 % H_2O) to effectively remove humidity-induced biases in isotopologue mole fractions and $\delta^{13}CH_4$. The observed water vapor dependencies were best represented by quadratic functions for $^{12}CH_4$ and $^{13}CH_4$, and a linear function for $\delta^{13}CH_4$. For $^{12}CH_4$ and $^{13}CH_4$, the residuals fell within the analyzer's precision, while $\delta^{13}CH_4$ residuals remained small and comparable to the precision. These water correction equations provide a robust basis for correcting field data. While most field systems employ physical air drying (e.g.,

Table 4. Regression results of concentration dependence of $\Delta\delta^{13}CH_4$ at Jurong (humid air) and SORPES (dry air) sites. $\Delta\delta^{13}CH_4$ is defined as the inter-method difference between isotopologue-specific and delta-based calibrated $\delta^{13}CH_4$ ($\Delta = \delta^{13}CH_4\_iso - \delta^{13}CH_4\_delta$). The dependence on CH_4 mole fraction was fitted using the function $\Delta = c0 + c1/CH_4 + c2CH_4$, where $c0$, $c1$, and $c2$ are regression coefficients (Griffth et al., 2018). All results are based on 5-min averaged data. *Significance levels*: $p < 0.05$ (*), $p < 0.01$ (**). The "Dominant term" column identifies whether the contribution of $c1$ or $c2$ is greater, based on their evaluated magnitudes at the median CH_4 mole fraction of each concentration range. Bold rows indicate the concentration subset containing the highest proportion of observations for each site, and thus the most representative range for that site.

Site, CH_4 mole fraction	Water conditions	Regression coefficients ($c0, c1, c2$)			Fit statistics	Number of	Dominant
(ppb, % of data)	(H_2O, %)	$c0$	$c1$ ($1/CH_4$, ppb)	$c2$ (CH_4, ppb)	(R^2, p)	data points (N)	term
Jurong, 2000–6000 (100 %)	Humid air:	6.85	-1.71×10^4	-4.13×10^{-4}	**0.23****	3119	$c1$, $1/CH_4$
Jurong, 2000–2500 (58.90 %)	(1.0 %–3.5 %)	**280.633**	$\mathbf{-3.36 \times 10^5}$	**−0.06**	**0.31****	**1837**	**c1, 1/CH$_4$**
Jurong, 2500–3000 (24.33 %)		−114.26	1.58×10^4	0.02	0.02	759	$c2$, CH_4
Jurong, 3000–3500 (8.85 %)		150.13	-2.56×10^5	−0.02	0.05	276	$c1$, $1/CH_4$
SORPES, 1800–3000 (100 %)	Dried air:	−15.08	3.33×10^4	7.46×10^{-5}	**0.78****	35 629	$c1$, CH_4
SORPES, 1500–2000 (3.08 %)	(< 0.1 %)	67.52	-5.09×10^{44}	−0.0199	0.07	1100	$c2$, CH_4
SORPES, 2000–2500 (93.86 %)		**1.57**	$\mathbf{1.42 \times 10^4}$	**−0.0035**	**0.73****	**33 442**	**c2, CH$_4$**
SORPES, 2500–3000 (3.05 %)		−9.05	2.42×10^4	−0.0009	0.66**	1087	$c1$, $1/CH_4$

Nafion™ dryers), residual H_2O often persists at levels sufficient to introduce measurable isotopic bias. Therefore, explicit humidity correction remains necessary, particularly under high-humidity conditions.

For dry air measurements, both calibration strategies yielded consistent $\delta^{13}CH_4$ results. Laboratory tests and dried-air observations at the SORPES site confirmed nearly identical retrievals between the two approaches, with a bias of 0.29 ‰, which is small but non-negligible relative to the extended compatibility goal (±0.2 ‰, $k = 2$) and comparable to our target-gas repeatability. In contrast, significant inter-method discrepancies emerged for humid air measurement. The bias ($\Delta\delta^{13}CH_4$) correlated strongly with both CH_4 and H_2O levels, indicating that humidity and concentration jointly modulate calibration accuracy. Consequently, the isotopologue-specific calibration method is better suited for accurate $\delta^{13}CH_4$ retrievals under conditions of fluctuating humidity and CH_4 concentrations.

The empirical water-vapor correction functions and calibration parameters reported here were derived for a single Picarro G2201-i analyzer and therefore should not be assumed to be directly transferable across instruments or deployments. Instrument-to-instrument differences (e.g., optical alignment, detector response, and aging) may lead to different humidity sensitivities and concentration dependences, so the empirical coefficients generally need to be re-derived and validated for each analyzer and field campaign over the relevant H_2O and CH_4 ranges. While the function and workflow are transferable, applying this framework to other instruments requires instrument-specific characterization using controlled humidity tests and routine reference-/target-gas checks.

Appendix A

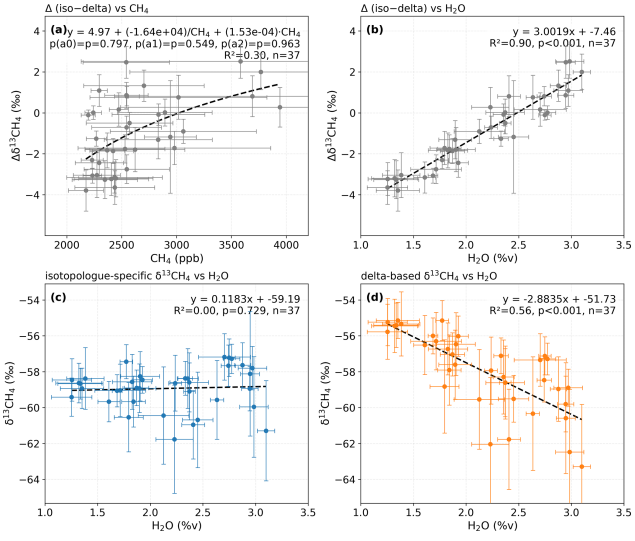

Figure A1. Correlations between $\delta^{13}CH_4$ calibration results and CH_4 and H_2O for humid air observations at the Jurong site. Relationship between **(a)** $\Delta\delta^{13}CH_4$ and CH_4; **(b)** $\Delta\delta^{13}CH_4$ and H_2O; **(c)** isotopologue-specific $\delta^{13}CH_4$ and H_2O; **(d)** delta-based $\delta^{13}CH_4$ and H_2O. Dashed lines indicate fitted regressions. The fitted equations, R^2, p, and n are reported in each panel.

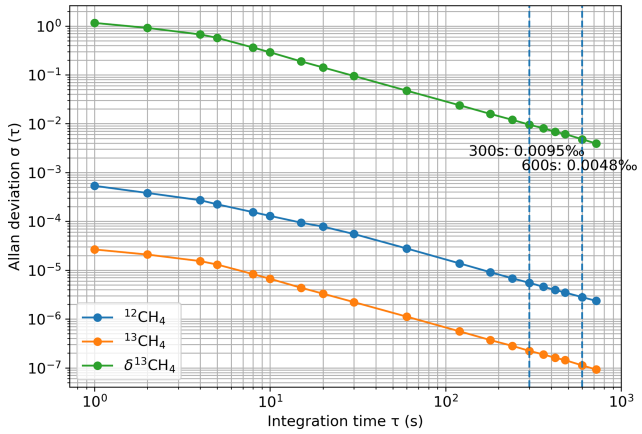

Figure A2. Allan deviation versus integration time for $^{12}CH_4$, $^{13}CH_4$, and $\delta^{13}CH_4$ from the Picarro G2201-i, calculated from a stable target-gas segment using 1 s data. Vertical lines mark $\tau = 300$ and 600 s.

Data availability. The data used in this study are available from the corresponding author upon reasonable request.

Author contributions. J.L. and H.C. conceived the study. J.L. performed the laboratory and field experiments, analyzed the data. X.C. and A.D., W.J., Y.Z., and J.C. provided scientific guidance for the field experiments. J.L. and H.C. wrote the manuscript with contributions from all authors.

Competing interests. At least one of the (co-)authors is a member of the editorial board of *Atmospheric Measurement Techniques*.

Disclaimer. Publisher's note: Copernicus Publications remains neutral with regard to jurisdictional claims made in the text, published maps, institutional affiliations, or any other geographical representation in this paper. The authors bear the ultimate responsibility for providing appropriate place names. Views expressed in the text are those of the authors and do not necessarily reflect the views of the publisher.

Special issue statement. This article is part of the special issue "Greenhouse gas monitoring in the Asia–Pacific region (ACP/AMT/GMD inter-journal SI)". It is a result of the 4th China Greenhouse Gas Monitoring Symposium, Nanjing, China, 2–3 November 2024.

Acknowledgements. The study was supported by the National Natural Science Foundation of China (grant numbers 42305129, 42475115, U24A20590), the Fundamental Research Funds for the Central Universities – Cemac "GeoX" Interdisciplinary Program (grant numbers 2024QNXZ01, 2024300245, 14380235). This work was supported by the project of Youth Crossdisciplinary Team of the Chinese Academy of Sciences (No. 2023000126). This research was also supported by the Collaborative Innovation Center of Climate Change, Jiangsu Province.

Financial support. The study was supported by the National Natural Science Foundation of China (grant nos. 42305129, 42475115, U24A20590), the Fundamental Research Funds for the Central Universities – Cemac "GeoX" Interdisciplinary Program (grant nos. 2024QNXZ01, 2024300245, 14380235). This work was supported by the project of Youth Crossdisciplinary Team of the Chinese Academy of Sciences (grant no. 2023000126). This research was also supported by the Collaborative Innovation Center of Climate Change, Jiangsu Province.

Review statement. This paper was edited by Andre Butz and reviewed by David Griffith and one anonymous referee.

References

Bakkaloglu, S., Lowry, D., Fisher, R. E., Menoud, M., Lanoisellé, M., Chen, H., Röckmann, T., and Nisbet, E. G.: Stable isotopic signatures of methane from waste sources through atmospheric measurements, Atmos. Environ., 276, 119021, https://doi.org/10.1016/j.atmosenv.2022.119021, 2022.

Berden, G. and Engeln, R.: Cavity ring-down spectroscopy: techniques and applications, John Wiley & Sons, https://doi.org/10.1002/9781444308259, 2009.

Braden-Behrens, J., Yan, Y., and Knohl, A.: A new instrument for stable isotope measurements of ^{13}C and ^{18}O in CO_2 – instrument performance and ecological application of the Delta Ray IRIS analyzer, Atmos. Meas. Tech., 10, 4537–4560, https://doi.org/10.5194/amt-10-4537-2017, 2017.

Chen, H., Winderlich, J., Gerbig, C., Hoefer, A., Rella, C. W., Crosson, E. R., Van Pelt, A. D., Steinbach, J., Kolle, O., Beck, V., Daube, B. C., Gottlieb, E. W., Chow, V. Y., Santoni, G. W., and Wofsy, S. C.: High-accuracy continuous airborne measurements of greenhouse gases (CO_2 and CH_4) using the cavity ring-down spectroscopy (CRDS) technique, Atmos. Meas. Tech., 3, 375–386, https://doi.org/10.5194/amt-3-375-2010, 2010.

Crosson, E.: A cavity ring-down analyzer for measuring atmospheric levels of methane, carbon dioxide, and water vapor, Appl. Phys. B, 92, 403–408, https://doi.org/10.1007/s00340-008-3135-y, 2008

Crosson, E. R., Ricci, K. N., Richman, B. A., Chilese, F. C., Owano, T. G., Provencal, R. A., Todd, M. W., Glasser, J., Kachanov, A. A., and Paldus, B. A.: Stable isotope ratios using cavity ring-down spectroscopy: determination of $^{13}C/^{12}C$ for carbon dioxide in human breath, Anal. Chem., 74, 2003–2007, https://doi.org/10.1021/ac025511d, 2002.

Defratyka, S. M., France, J. L., Fisher, R. E., Lowry, D., Fernandez, J. M., Bakkaloglu, S., Yver-Kwok, C., Paris, J.-D., Bousquet, P., and Arnold, T.: Evaluation of data processing strategies for methane isotopic signatures determined during near-source measurements, Tellus B, 77, https://doi.org/10.16993/tellusb.1878, 2025.

De Groot, P. A.: Handbook of stable isotope analytical techniques, Elsevier, https://www.sciencedirect.com/science/book/9780444511140 (last access: 9 March 2026), 2004.

Ding, A., Nie, W., Huang, X., Chi, X., Sun, J., Kerminen, V.-M., Xu, Z., Guo, W., Petäjä, T., Yang, X., Kulmala, M., and Fu, C.: Long-term observation of air pollution–weather/climate interactions at the SORPES station: a review and outlook, Frontiers of Environmental Science & Engineering, 10, 15, https://doi.org/10.1007/s11783-016-0877-3, 2016.

Ehleringer, J. R. and Osmond, C. B.: Stable isotopes, in: Plant physiological ecology: field methods and instrumentation, Springer, 281–300, https://doi.org/10.1007/978-94-009-2221-1, 1989.

Flores, E., Viallon, J., Moussay, P., Griffith, D. W., and Wielgosz, R. I.: Calibration strategies for FT-IR and other isotope ratio infrared spectrometer instruments for accurate $\delta^{13}C$ and $\delta^{18}O$ measurements of CO_2 in air, Anal. Chem., 89, 3648–3655, https://doi.org/10.1021/acs.analchem.6b05063, 2017.

Forster, P., Storelvmo, T., Armour, K., Collins, W., Dufresne, J.-L., Frame, D., Lunt, D., Mauritsen, T., Palmer, M., and Watanabe, M.: The Earth's energy budget, climate feedbacks, and climate sensitivity, in: Climate Change 2021: The Physical Science Basis. Contribution of Working Group I to the Sixth Assessment Report of the Intergovernmental Panel on Climate Change, Cambridge University Press, pp. 923–1054, https://doi.org/10.1017/9781009157896.009, 2021.

France, J. L., Fisher, R. E., Lowry, D., Allen, G., Andrade, M. F., Bauguitte, S. J.-B., Bower, K., Broderick, T. J., Daly, M. C., and Forster, G.: $\delta^{13}C$ methane source signatures from tropical wetland and rice field emissions, Philos. T. R. Soc. A, 380, 20200449, https://doi.org/10.1098/rsta.2020.0449, 2022.

Griffith, D. W. T.: Calibration of isotopologue-specific optical trace gas analysers: a practical guide, Atmos. Meas. Tech., 11, 6189–6201, https://doi.org/10.5194/amt-11-6189-2018, 2018.

Griffith, D. W. T., Deutscher, N. M., Caldow, C., Kettlewell, G., Riggenbach, M., and Hammer, S.: A Fourier transform infrared trace gas and isotope analyser for atmospheric applications, Atmos. Meas. Tech., 5, 2481–2498, https://doi.org/10.5194/amt-5-2481-2012, 2012.

Hoheisel, A., Yeman, C., Dinger, F., Eckhardt, H., and Schmidt, M.: An improved method for mobile characterisation of $\delta^{13}CH_4$ source signatures and its application in Germany, Atmos. Meas. Tech., 12, 1123–1139, https://doi.org/10.5194/amt-12-1123-2019, 2019.

IAEA: Measurement of the stable carbon isotope ratio in atmospheric CH_4 using laser spectroscopy for CH_4 source characterization, IAEA Pan. P., https://doi.org/10.61092/iaea.logm-wiux, 2024.

IPCC: Climate Change 2007: The Physical Science Basis. Contribution of Working Group I to the Fourth Assessment Report of the Intergovernmental Panel on Climate Change, Cambridge University Press, Cambridge, United Kingdom and New York, NY, USA, 996 pp., https://wedocs.unep.org/20.500.11822/30763 (last access: 9 March 2026), 2007.

Kirschke, S., Bousquet, P., Ciais, P., Saunois, M., Canadell, J. G., Dlugokencky, E. J., Bergamaschi, P., Bergmann, D., Blake, D. R., and Bruhwiler, L.: Three decades of global methane sources and sinks, Nat. Geosci., 6, 813–823, https://doi.org/10.1038/ngeo1955, 2013.

Lan, X., Basu, S., Schwietzke, S., Bruhwiler, L. M., Dlugokencky, E. J., Michel, S. E., Sherwood, O. A., Tans, P. P., Thoning, K., and Etiope, G.: Improved constraints on global methane emissions and sinks using $\delta^{13}CH_4$, Global Biogeochem. Cy., 35, e2021GB007000, https://doi.org/10.1029/2021GB007000, 2021.

Levin, I., Bergamaschi, P., Dörr, H., and Trapp, D.: Stable isotopic signature of methane from major sources in Germany, Chemosphere, 26, 161–177, https://doi.org/10.1016/0045-6535(93)90419-6, 1993.

Li, J., Zhang, Y., Gu, L., Li, Z., Li, J., Zhang, Q., Zhang, Z., and Song, L.: Seasonal variations in the relationship between sun-induced chlorophyll fluorescence and photosynthetic capacity from the leaf to canopy level in a rice crop, J. Exp. Bot., 71, 7179–7197, https://doi.org/10.1093/jxb/eraa408, 2020.

Miles, N. L., Martins, D. K., Richardson, S. J., Rella, C. W., Arata, C., Lauvaux, T., Davis, K. J., Barkley, Z. R., McKain, K., and Sweeney, C.: Calibration and field testing of cavity ring-down laser spectrometers measuring CH_4, CO_2, and $\delta^{13}CH_4$ deployed on towers in the Marcellus Shale region, Atmos. Meas. Tech., 11, 1273–1295, https://doi.org/10.5194/amt-11-1273-2018, 2018.

Miller, J. B., Mack, K. A., Dissly, R., White, J. W., Dlugokencky, E. J., and Tans, P. P.: Development of analytical methods and measurements of $^{13}C/^{12}C$ in atmospheric CH_4 from the NOAA Climate Monitoring and Diagnostics Laboratory global air sampling network, J. Geophys. Res.-Atmos., 107, ACH11-11–ACH11-15, https://doi.org/10.1029/2001JD000630, 2002.

Nisbet, E., Dlugokencky, E., Manning, M., Lowry, D., Fisher, R., France, J., Michel, S., Miller, J., White, J., and Vaughn, B.: Rising atmospheric methane: 2007–2014 growth and isotopic shift, Global Biogeochem. Cy., 30, 1356–1370, https://doi.org/10.1002/2016gb005406, 2016.

Nisbet, E., Fisher, R., Lowry, D., France, J., Allen, G., Bakkaloglu, S., Broderick, T., Cain, M., Coleman, M., and Fernandez, J.: Methane mitigation: methods to reduce emissions, on the path to the Paris agreement, Rev. Geophys., 58, e2019RG000675, https://doi.org/10.1029/2019RG000675, 2020.

Olivier, J. G. and Berdowski, J. J.: Global emission sources and sinks, in: The climate system, CRC Press, 33–77, https://doi.org/10.1201/9781003211266, 2021.

Pang, J., Wen, X., Sun, X., and Huang, K.: Intercomparison of two cavity ring-down spectroscopy analyzers for atmospheric $^{13}CO_2/^{12}CO_2$ measurement, Atmos. Meas. Tech., 9, 3879–3891, https://doi.org/10.5194/amt-9-3879-2016, 2016.

Patra, P. K. and Khatri, P.: Atmospheric mixing ratio of greenhouse gases and radiative forcing, in: Handbook of Air Quality and Climate Change, Springer, 1–29, https://doi.org/10.1007/978-981-15-2527-8_29-1, 2022.

Paul, D., Scheeren, H. A., Jansen, H. G., Kers, B. A. M., Miller, J. B., Crotwell, A. M., Michel, S. E., Gatti, L. V., Domingues, L. G., Correia, C. S. C., Neves, R. A. L., Meijer, H. A. J., and Peters, W.: Evaluation of a field-deployable Nafion™-based air-drying system for collecting whole air samples and its application to stable isotope measurements of CO_2, Atmos. Meas. Tech., 13, 4051–4064, https://doi.org/10.5194/amt-13-4051-2020, 2020.

Quay, P., Stutsman, J., Wilbur, D., Snover, A., Dlugokencky, E., and Brown, T.: The isotopic composition of atmospheric methane, Global Biogeochem. Cy., 13, 445–461, https://doi.org/10.1029/1998GB900006, 1999.

Rella, C.: Accurate stable carbon isotope ratio measurements in humid gas streams using the Picarro $\delta^{13}CO_2$ G2101-i gas analyzer, White Paper of Picarro Inc., 1–13, https://www.picarro.com/sites/default/files/product_documents/White_Paper_G2101-i_Water_Correction.pdf (last access: 9 March 2026), 2012.

Rella, C. W., Chen, H., Andrews, A. E., Filges, A., Gerbig, C., Hatakka, J., Karion, A., Miles, N. L., Richardson, S. J., Steinbacher, M., Sweeney, C., Wastine, B., and Zellweger, C.: High accuracy measurements of dry mole fractions of carbon dioxide and methane in humid air, Atmos. Meas. Tech., 6, 837–860, https://doi.org/10.5194/amt-6-837-2013, 2013.

Rella, C. W., Hoffnagle, J., He, Y., and Tajima, S.: Local- and regional-scale measurements of CH_4, $\delta^{13}CH_4$, and C2H6 in the Uintah Basin using a mobile stable isotope analyzer, Atmos. Meas. Tech., 8, 4539–4559, https://doi.org/10.5194/amt-8-4539-2015, 2015.

Rice, A. L., Butenhoff, C. L., Teama, D. G., Röger, F. H., Khalil, M. A. K., and Rasmussen, R. A.: Atmospheric methane isotopic record favors fossil sources flat in 1980s and 1990s with recent increase, P. Natl. Acad. Sci. USA, 113, 10791–10796, https://doi.org/10.1073/pnas.1522923113, 2016.

Röckmann, T., Eyer, S., van der Veen, C., Popa, M. E., Tuzson, B., Monteil, G., Houweling, S., Harris, E., Brunner, D., Fischer, H., Zazzeri, G., Lowry, D., Nisbet, E. G., Brand, W. A., Necki, J. M., Emmenegger, L., and Mohn, J.: In situ observations of the isotopic composition of methane at the Cabauw tall tower site, Atmos. Chem. Phys., 16, 10469–10487, https://doi.org/10.5194/acp-16-10469-2016, 2016.

Saboya, E., Zazzeri, G., Graven, H., Manning, A. J., and Englund Michel, S.: Continuous CH_4 and $\delta^{13}CH_4$ measurements in London demonstrate under-reported natural gas leakage, Atmos. Chem. Phys., 22, 3595–3613, https://doi.org/10.5194/acp-22-3595-2022, 2022.

Saunois, M., Stavert, A. R., Poulter, B., Bousquet, P., Canadell, J. G., Jackson, R. B., Raymond, P. A., Dlugokencky, E. J., Houweling, S., Patra, P. K., Ciais, P., Arora, V. K., Bastviken, D., Bergamaschi, P., Blake, D. R., Brailsford, G., Bruhwiler, L., Carlson, K. M., Carrol, M., Castaldi, S., Chandra, N., Crevoisier, C., Crill, P. M., Covey, K., Curry, C. L., Etiope, G., Frankenberg, C., Gedney, N., Hegglin, M. I., Höglund-Isaksson, L., Hugelius, G., Ishizawa, M., Ito, A., Janssens-Maenhout, G., Jensen, K. M., Joos, F., Kleinen, T., Krummel, P. B., Langenfelds, R. L., Laruelle, G. G., Liu, L., Machida, T., Maksyutov, S., McDonald, K. C., McNorton, J., Miller, P. A., Melton, J. R., Morino, I., Müller, J., Murguia-Flores, F., Naik, V., Niwa, Y., Noce, S., O'Doherty, S., Parker, R. J., Peng, C., Peng, S., Peters, G. P., Prigent, C., Prinn, R., Ramonet, M., Regnier, P., Riley, W. J., Rosentreter, J. A., Segers, A., Simpson, I. J., Shi, H., Smith, S. J., Steele, L. P., Thornton, B. F., Tian, H., Tohjima, Y., Tubiello, F. N., Tsuruta, A., Viovy, N., Voulgarakis, A., Weber, T. S., van Weele, M., van der Werf, G. R., Weiss, R. F., Worthy, D., Wunch, D., Yin, Y., Yoshida, Y., Zhang, W., Zhang, Z., Zhao, Y., Zheng, B., Zhu, Q., Zhu, Q., and Zhuang, Q.: The Global Methane Budget 2000–2017, Earth Syst. Sci. Data, 12, 1561–1623, https://doi.org/10.5194/essd-12-1561-2020, 2020.

Saunois, M., Martinez, A., Poulter, B., Zhang, Z., Raymond, P. A., Regnier, P., Canadell, J. G., Jackson, R. B., Patra, P. K., Bousquet, P., Ciais, P., Dlugokencky, E. J., Lan, X., Allen, G. H., Bastviken, D., Beerling, D. J., Belikov, D. A., Blake, D. R., Castaldi, S., Crippa, M., Deemer, B. R., Dennison, F., Etiope, G., Gedney, N., Höglund-Isaksson, L., Holgerson, M. A., Hopcroft, P. O., Hugelius, G., Ito, A., Jain, A. K., Janardanan, R., Johnson, M. S., Kleinen, T., Krummel, P. B., Lauerwald, R., Li, T., Liu, X., McDonald, K. C., Melton, J. R., Mühle, J., Müller, J., Murguia-Flores, F., Niwa, Y., Noce, S., Pan, S., Parker, R. J., Peng, C., Ramonet, M., Riley, W. J., Rocher-Ros, G., Rosentreter, J. A., Sasakawa, M., Segers, A., Smith, S. J., Stanley, E. H., Thanwerdas, J., Tian, H., Tsuruta, A., Tubiello, F. N., Weber, T. S., van der Werf, G. R., Worthy, D. E. J., Xi, Y., Yoshida, Y., Zhang, W., Zheng, B., Zhu, Q., Zhu, Q., and Zhuang, Q.: Global Methane Budget 2000–2020, Earth Syst. Sci. Data, 17, 1873–1958, https://doi.org/10.5194/essd-17-1873-2025, 2025.

Schaefer, H., Whiticar, M. J., Brook, E. J., Petrenko, V. V., Ferretti, D. F., and Severinghaus, J. P.: Ice record of $\delta^{13}C$ for atmospheric CH_4 across the Younger Dryas–Preboreal transition, Science, 313, 1109–1112, https://doi.org/10.1126/science.1126562, 2006.

Schaefer, H., Fletcher, S. E. M., Veidt, C., Lassey, K. R., Brailsford, G. W., Bromley, T. M., Dlugokencky, E. J., Michel, S. E., Miller, J. B., and Levin, I.: A 21st-century shift from fossil-fuel to biogenic methane emissions indicated by $^{13}CH_4$, Science, 352, 80–84, https://doi.org/10.1126/science.aad2705, 2016.

Shindell, D., Kuylenstierna, J. C., Vignati, E., van Dingenen, R., Amann, M., Klimont, Z., Anenberg, S. C., Muller, N., Janssens-Maenhout, G., and Raes, F.: Simultaneously mitigating near-term climate change and improving human health and food security, Science, 335, 183–189, https://doi.org/10.1126/science.1210026, 2012.

Tans, P. P., Crotwell, A. M., and Thoning, K. W.: Abundances of isotopologues and calibration of CO_2 greenhouse gas measurements, Atmos. Meas. Tech., 10, 2669–2685, https://doi.org/10.5194/amt-10-2669-2017, 2017.

Tuzson, B., Mohn, J., Zeeman, M. J., Werner, R. A., Eugster, W., Zahniser, M. S., Nelson, D. D., McManus, J. B., and Emmenegger, L.: High precision and continuous field measurements of $\delta^{13}C$ and $\delta^{18}O$ in carbon dioxide with a cryogen-free QCLAS, Appl. Phys. B, 92, 451–458, https://doi.org/10.1007/s00340-008-3085-4, 2008.

Van Dingenen, R., Crippa, M., Maenhout, G., Guizzardi, D., and Dentener, F.: Global trends of methane emissions and their impacts on ozone concentrations, JRC Science for Policy Report, JRC113210, ISBN 978-92-79-96550-0, https://doi.org/10.2760/820175, 2018.

Wahl, E. H., Fidric, B., Rella, C. W., Koulikov, S., Kharlamov, B., Tan, S., Kachanov, A. A., Richman, B. A., Crosson, E. R., and Paldus, B. A.: Applications of cavity ring-down spectroscopy to high precision isotope ratio measurement of $^{13}C/^{12}C$ in carbon dioxide, Isot. Environ. Healt. S., 42, 21–35, https://doi.org/10.1080/10256010500502934, 2006.

Welp, L. R., Keeling, R. F., Weiss, R. F., Paplawsky, W., and Heckman, S.: Design and performance of a Nafion dryer for continuous operation at CO_2 and CH_4 air monitoring sites, Atmos. Meas. Tech., 6, 1217–1226, https://doi.org/10.5194/amt-6-1217-2013, 2013.

Wen, X.-F., Meng, Y., Zhang, X.-Y., Sun, X.-M., and Lee, X.: Evaluating calibration strategies for isotope ratio infrared spectroscopy for atmospheric $^{13}CO_2/^{12}CO_2$ measurement, Atmos.

Meas. Tech., 6, 1491–1501, https://doi.org/10.5194/amt-6-1491-2013, 2013.

Werner, R. A. and Brand, W. A.: Referencing strategies and techniques in stable isotope ratio analysis, Rapid Commun. Mass Sp., 15, 501–519, https://doi.org/10.1002/rcm.258, 2001.